ARTICLE

Tailoring exciton dynamics of monolayer transition metal dichalcogenides by interfacial electron-phonon coupling

Zhonghui Nie[1,2,5], Yongliang Shi[3,5], Shuchao Qin[1,2,5], Yuhan Wang[1,2], Hongzhu Jiang[1,2], Qijing Zheng [3], Yang Cui[1], Yuze Meng[4], Fengqi Song[4], Xiaoyong Wang[4], Ion C.E. Turcu[1], Xinran Wang [1], Yongbing Xu[1], Yi Shi [1], Jin Zhao [3], Rong Zhang[1] & Fengqiu Wang [1,2]

With their strong light-matter interaction and rich photo-physics, two-dimensional (2D) transition metal dichalcogenides (TMDs) are important candidates for novel photonic and spin-valleytronic devices. It is highly desirable to control the photocarrier behaviours of monolayer TMDs to suit the needs of device functionalities. Here, through interfacial engineering, i.e., by depositing monolayer $MoSe_2$ onto different oxide substrates (SiO_2, Al_2O_3 and HfO_2), we have revealed large tuning of the exciton relaxation times in monolayer TMDs. Significantly, the non-radiative recombination of $MoSe_2$ is found shortened by almost one order of magnitude, from 160 ± 10 ps (on SiO_2) to 20 ± 4 ps (on HfO_2). Theoretical simulations based on ab initio non-adiabatic molecular dynamics (NAMD) method, together with temperature-dependent optical spectroscopy, identifies interfacial electron-phonon (e-ph) coupling as the leading mechanism for the lifetime tuning. Our results establish interface engineering as an effective knob for manipulating excited-state dynamics of monolayer TMDs.

[1] School of Electronic Science and Engineering and Collaborative Innovation Center of Advanced Microstructures, Nanjing University, Nanjing 210093, China. [2] Key Laboratory of Intelligent Optical Sensing and Manipulation, Ministry of Education, Nanjing University, Nanjing 210093, China. [3] ICQD/Hefei National Laboratory for Physical Sciences at Microscale, and Key Laboratory of Strongly-Coupled Quantum Matter Physics, Chinese Academy of Sciences, and Department of Physics, University of Science and Technology of China, Hefei, Anhui 230026, China. [4] National Laboratory of Solid State Microstructures and School of Physics, Nanjing University, Nanjing 210093, China. [5] These authors contributed equally: Zhonghui Nie, Yongliang Shi, Shuchao Qin. Correspondence and requests for materials should be addressed to J.Z. (email: zhaojin@ustc.edu.cn) or to R.Z. (email: rzhang@nju.edu.cn) or to F.W. (email: fwang@nju.edu.cn)

Monolayer transition metal dichalcogenides (TMDs), one of the most widely studied two-dimensional (2D) semiconductors, have attracted significant attention and are deemed an ideal platform to construct next generation nanodevices, thanks to its unique electrical, optical, and spin-valleytronic properties[1–4]. In particular, due to their strong quantum confinement and enhanced Coulomb interaction[2,5–7], monolayer TMDs support robust excitons with binding energies in excess of hundreds of meV[8]. The prospect of having high quantum yield[9] as well as flexible doping control[10] makes monolayer TMDs appealing for a range of photonic devices, such as photodetectors[11], light-emitting diodes[12,13], and optical modulators[14]. For photonic device applications, several important figures-of-merit are closely linked to photocarrier dynamics[15–20], and the ability to customize the photocarrier lifetimes would make TMDs highly adaptable to various application scenarios. To this end, ultrafast pump-probe investigations of monolayer TMDs have been extensively reported[15–24], however, a robust approach that can tailor the exciton dynamics of monolayer TMDs, while maintaining compatibility with large-scale device fabrication, is still lacking.

For conventional semiconductor materials, e.g., III–V compound GaAs, a number of techniques developed during the 1990s are available for controlling the photocarrier dynamics, among which inducing lattice defects through low-temperature growth or ion implantation had proved particularly effective[25,26]. Combined with post-growth annealing, these techniques have made time constants tuneable from nanoseconds down to ~100 fs range, making GaAs a highly versatile base material for ultrafast optoelectronics[27]. Unfortunately, techniques for photocarrier dynamics tuning developed for bulk semiconductors cannot be straightforwardly applied to 2D systems as hindered by their atomically thin nature. Developing new and generic approaches that can be employed to modulate photocarrier/exciton behaviours in 2D semiconductors is of both fundamental importance and practical relevance[28]. Interlayer electron (excitons)–phonon (e–ph) coupling has emerged as a mechanism that directly impacts carrier transport in 2D materials, e.g., it sets the limit of electron mobility in graphene[29]. Recently, several pioneering works uncovered a new form of interlayer e–ph coupling at van der Waals interfaces formed by TMD/hBN or TMD/dielectric substrates[30–32]. Specifically, it was found that in WSe$_2$/hBN heterostructures, optical silent hBN phonon modes can be activated by resonant coupling with electronic transitions (or excitons) of WSe$_2$ and it is notable that the coupling with phonons from the dielectric substrates are particularly strong[30–32]. The existence of interfacial e–ph coupling between TMDs and adjacent dielectric layers offers a potentially viable route for tailoring the transient optical properties of low-dimensional systems and also realize novel quantum phenomena unobserved before[30–32].

Here, we investigate the exciton dynamics of monolayer MoSe$_2$ deposited on three dielectric substrates (SiO$_2$, Al$_2$O$_3$, and HfO$_2$) with different dielectric and phononic properties. Surprisingly, the substrates are found to strongly affect the exciton relaxation times of monolayer MoSe$_2$ (from ~160 ps on SiO$_2$ to ~20 ps on HfO$_2$). Time-resolved photoluminescence (TR-PL) suggests that such a modulating effect primarily impacts the non-radiative relaxation channels. We attribute the lifetime tuning to interlayer e–ph coupling, as conceptually illustrated in Fig. 1a, where the vibration modes (denoted by the ball pairs) of the substrate lattices can couple with the excitons (red and blue ellipses) in MoSe$_2$, offering an efficient route for exciton energy dissipation. Theoretical simulations, based on ab initio non-adiabatic molecular dynamics (NAMD) approach, reproduce qualitatively similar results. We further elucidate the different effects of interfacial e–ph coupling by corroborating the photo-generated exciton lifetime with transport measurements in a MoS$_2$ based field-effect transistor, where enhanced charge-carrier mobility and reduced exciton lifetime are observed simultaneously. Our finding suggests that interfacial engineering can be a promising way to modulate photocarrier dynamics in atomically thin semiconductors without compromising the intrinsic electrical properties of 2D materials. It represents a step forward in promoting TMDs as a superior and versatile base material for next generation 2D optoelectronics.

Results

Photocarrier dynamics of monolayer MoSe$_2$ on different substrates. Chemical vapor deposition (CVD)-grown monolayer MoSe$_2$ was transferred onto different oxide substrates (SiO$_2$, Al$_2$O$_3$ and HfO$_2$), through a dry transfer process (details in Methods). The thickness of the oxide layers was intentionally made thin (~30 nm), much smaller than the laser wavelengths, so that optical interference effect associated with the substrates' geometrical features can be safely ignored. PL and Raman spectra, shown in Supplementary Figs. 1a, b and 2, confirm good quality of samples on different substrates[33,34]. In addition, the atomic force microscopy (AFM) images of samples on different substrates, as illustrated in Supplementary Fig. 1c–e, reveal a layer thickness of ~0.8 nm, consistent with previous reports on monolayer MoSe$_2$[5,33,34], and confirm that there is no gap between the samples and substrates. These results prove that transferring onto different substrates has negligible impact on the integrity of the samples.

Ultrafast spectroscopy was carried out using a pump-probe setup (details in Methods and Supplementary Fig. 3). First, we investigated the photocarrier dynamics at the A-exciton resonance. Figure 1b summarizes the normalized transient reflectance signals from the three different samples, with a pump wavelength of 400 nm (3.1 eV) and a probe wavelength of 800 nm (1.55 eV). The absorption coefficient of monolayer MoSe$_2$ at the pump wavelength is ~8×10^5 cm^{-1} (ref. [35]). Assuming each pump photon absorbed excites one pair of electron and hole, a peak photocarrier density of ~1.7×10^{11} cm^{-2} is injected, where the nonlinear effects induced by high carrier density are expected to be avoided[21]. Dynamical curves exhibit an instantaneous rise within 400 fs, as defined by our instrument response. All transient reflectivity curves exhibit three temporal stages, the exact origins of which will be discussed later. In this work, we mainly focus on the longest recombination time constant (denoted by τ_3), as it is generally taken as the overall response time of the material in the context of device applications. While the MoSe$_2$/SiO$_2$ sample shows a recombination time of few hundreds of picoseconds, similar with previous reports[17,19], the relaxation times of monolayer MoSe$_2$ on the other two substrates are appreciably shorter. Specifically, τ_3 is seen to reduce from 160 ± 10 ps on SiO$_2$ to 73 ± 7 ps on Al$_2$O$_3$, and to 20 ± 4 ps on HfO$_2$. To make sure the salient difference in the recombination dynamics are indeed caused by the substrates, different flakes on the same substrate and multiple positions on the same flake were further measured (Supplementary Fig. 4) and the results are well reproducible and consistent, ruling out major contribution from the variation in the growth and transfer process. In addition, the fluence-independent dynamics (Supplementary Fig. 5) helps to exclude the effect of exciton density on our main observations.

Before moving to probe the mechanism for the significant modulation of τ_3, we briefly discuss the observations about the first two relaxation components. The measured initial fast relaxation time τ_1 of monolayer MoSe$_2$ on different substrates is summarized in Supplementary Fig. 6 and stays almost constant (~400–500 fs) for all samples. Such short relaxation time could
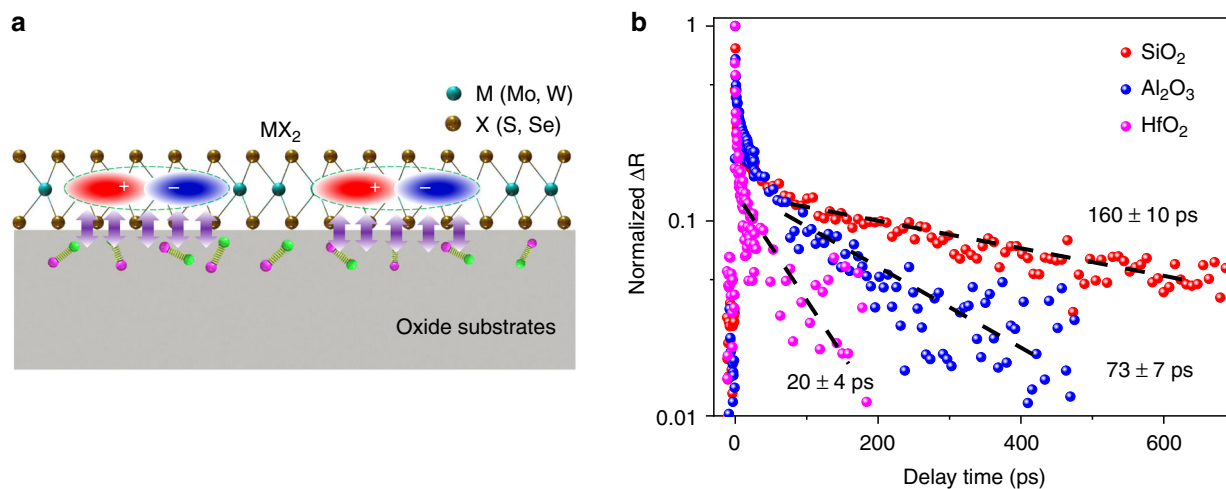
Fig. 1 Ultrafast photocarrier dynamics of monolayer MoSe$_2$ on different oxide substrates. **a** Illustration of interfacial electron–phonon (e–ph) coupling; electrons (excitons) in monolayer TMDs and surface phonons from oxide layers are shown and the purple arrows represent the interaction between excitons and phonons. **b** Photocarrier dynamics of monolayer MoSe$_2$ on different substrates and black dashed lines represent the exponential fitting to the last relaxation component, where the corresponding relaxation times are also exhibited

originate from the initial process, related to hot carriers[17,36–38]. Considering the fluence-independent dynamics (Supplementary Fig. 5) and ultrafast hot carrier interactions, we assign this sub-picosecond decay to carrier–carrier interaction, which leads to the formation of excitons from photo-excited free carriers (See Supplementary Note 1). Similar results have been observed in other TMDs and addressed by both theory and experiments[37–39]. With regard to the second relaxation time τ_2, a slight dependence on substrate type is discernible, and the timescale indicates that the second relaxation stage is primarily associated with exciton–exciton annihilation (EEA), a classical many-body effect that leads to fast reduction of exciton population. Such a process is typically found dominant before 50 ps and depends mildly on the surrounding environments[40,41], as shown in Supplementary Fig. 7 (see Supplementary Note 2).

To gain more physical insights into the observed tuning of the overall recombination time τ_3 via substrate engineering, which has not been observed before, we then inspected the possible influence of substrates on exciton configurations and the radiative channel. It is known that the dielectric screening effect from the surrounding environment can cause bandgap renormalization and reduction of excitonic binding energy, leading to changes of excitonic configuration and PL lifetime of monolayer TMDs[8,33,42]. TR-PL spectra were measured by a streak-camera-based setup (with a time resolution of ~32 ps), as shown in Fig. 2a. No obvious modulation of the radiative lifetime is present, and a nearly constant PL lifetime of ~600–700 ps is obtained, agreeing with previous results[43]. The nearly constant PL lifetimes indicate that the binding states of excitons on different substrates should be similar, since radiative lifetime is directly related with the binding energy and susceptible to the dielectric screening effect (see details in Supplementary Note 3)[44]. Therefore, the TR-PL results could help to rule out the dielectric screening effect as dominant effect in our case, and also suggest that the relatively slow relaxation time τ_3 can be attributed to the non-radiative recombination of excitons in monolayer MoSe$_2$, which is typically mediated by defects in TMDs, especially for CVD-grown samples. In addition, as it has been reported that the dielectric screening of Coulomb interaction could result in appreciable shift of PL peak positions[33,42], the consistent excitonic states of the three samples evidenced by the slight variance in PL peak positions (shown in Fig. S2) also indicate that the difference in dielectric screening by

the substrates is minor and should not the main cause of the observed large variance in the photocarrier dynamics.

With the dielectric screening effect being excluded, we continued to investigate potential mechanisms of the exciton lifetime tuning through performing non-degenerate pump-probe characterization over an extended probe wavelength range from ~765–810 nm (1.62–1.53 eV) as illustrated in Fig. 2b. As before, the pump photon energy was twice that of the probe using a second-harmonic generation (SHG) setup. It is clearly seen that the strong influence of the substrates still prevails, indicating this effect is largely independent of probing wavelengths (Supplementary Fig. 8). Such broadband and robust effect on the non-radiative recombination prompts us to examine the likely roles of e–ph coupling. To verify the role of phonons in the process, we measured temperature-dependent transient spectroscopy. As temperature was lowered from room temperate to ~80 K, we observed a drastically elongated relaxation time constant τ_3 (For Al$_2$O$_3$ substrate, the value of τ_3 changes from under 60 ps to over 800 ps), as shown in Fig. 2c. Such a temperature dependence strongly indicates that a phonon-assisted process is associated with the long-lived recombination lifetime τ_3. Low-temperature TR-PL was also carried out and again for the three samples, no modulation of radiative lifetimes is detected, as seen in Fig. 2d. Based on the experimental evidence above, we infer that different contribution from phonons provided by oxide substrates could be the primary mechanism for the unusual long-range tuning of the non-radiative electron–hole (e–h) recombination lifetime.

Theoretical simulation of recombination dynamics on different substrates. To verify our analysis, theoretical calculations were carried out using the ab initio NAMD approach to simulate the non-radiative e–h recombination within the framework of time-dependent density functional theory (TDDFT) combined with fewest switches surface hopping (FSSH) scheme (Supplementary Fig. 9)[45–47]. In this method, the time-dependent wave function is expanded using a set of adiabatic Kohn–Sham (KS) orbitals for each configuration during the ab initio molecular dynamics. The evolution of the Hamiltonian follows the time-dependent KS equation. In addition, the excited carrier can hop from one KS orbital to another, in which the hopping probability is determined by the non-adiabatic coupling (NAC) elements
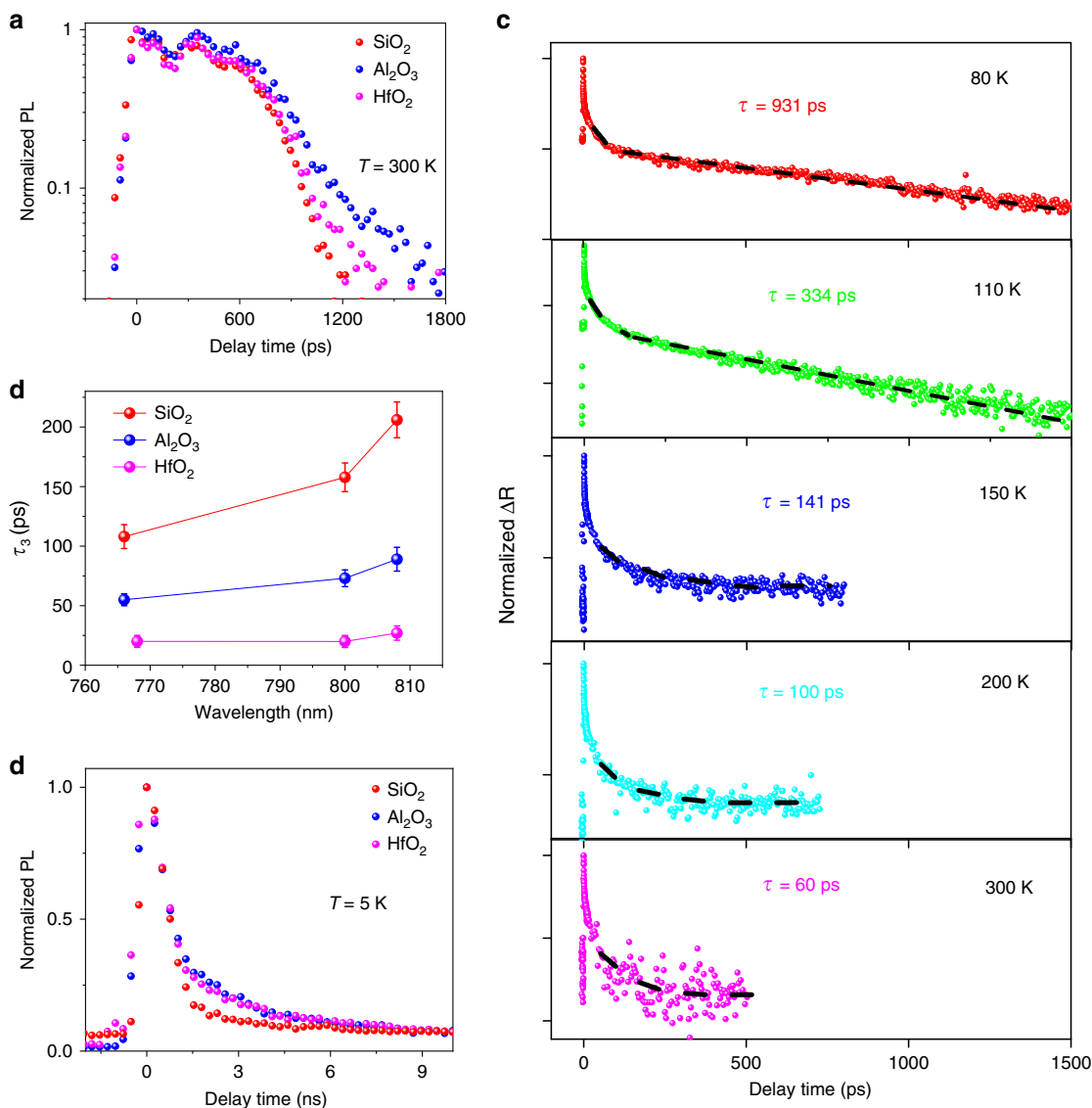
3

Fig. 2 Temperature dependence of photoluminescence (PL) lifetime and photocarrier dynamics of monolayer MoSe₂ on different oxide substrates. a Time-resolved photoluminescence (TR-PL) of the three samples under room temperature, and the corresponding lifetimes are ~700 ps; **b** the last relaxation time τ_3 of samples on different substrates as a function of probe wavelength. The error bars represent the standard deviation from multiple measurements; **c** transient reflectance signals of monolayer MoSe₂ on Al₂O₃ under different temperatures varying from 80 to 300 K. Black dashed lines represent fitting on the third relaxation component and the corresponding relaxation times are also labelled; **d** TR-PL signals at low temperature (5 K) and the lifetimes for all the samples are ~1 ns

between different KS orbitals (see Supplementary Note 4). Such method has been successfully applied to describe the non-radiative e–h recombination dynamics in 2D materials[20,48].

As shown in Fig. 3a–c, the e–h recombination in MoSe₂ exhibits distinct behaviors on three different substrates. The e–h recombination timescale can be estimated by fitting the time-dependent electron population using an exponential function, which are 34, 51 and 155 ps for MoSe₂ on HfO₂, Al₂O₃ and SiO₂, respectively. Although this NAMD method based on single particle does not account for the excitonic effect, which could lead to the deviation between the experimental lifetimes and simulated ones, the trend of lifetime variation obtained from the numerical calculations agrees well with the experimental observation. Considering the similar excitonic states as suggested by the PL and TR-PL characterization, the excitonic effect should not be responsible for the observed excition lifetime tuning and the consistent trend of lifetime variation in experiment and simulation also confirmed that the simplied model applied here

shoud be adequate to identify the dominat physical mechanism on the lifetime tuning in these TMDs-oxide systems. Trying to understand this distinction, we plotted out the averaged NAC elements which determine the hopping probability of excited e/h between different energy states in NAMD simulations (Supplementary Fig. 10). As mentioned above, larger NACs represent higher hopping probabilities of carriers between the adiabatic KS states and thus shorter e–h recombination time. NACs can be calculated as:

$$d_{jk} = \left\langle \boldsymbol{\varphi}_j \left| \frac{\partial}{\partial t} \right| \boldsymbol{\varphi}_k \right\rangle = \frac{\left\langle \boldsymbol{\varphi}_j | \nabla_R H | \boldsymbol{\varphi}_k \right\rangle}{\epsilon_k - \epsilon_j} \dot{\mathbf{R}} \qquad (1)$$

In Eq. (1), H is the Kohn–Sham Hamiltonian, $\boldsymbol{\varphi}_j$, $\boldsymbol{\varphi}_k$, ϵ_j, ϵ_k are the corresponding wave functions and eigenvalues for electronic states j and k, and $\dot{\mathbf{R}}$ is velocity of the nuclei. From Eq. (1), one can see that the NAC elements show strong dependence on the
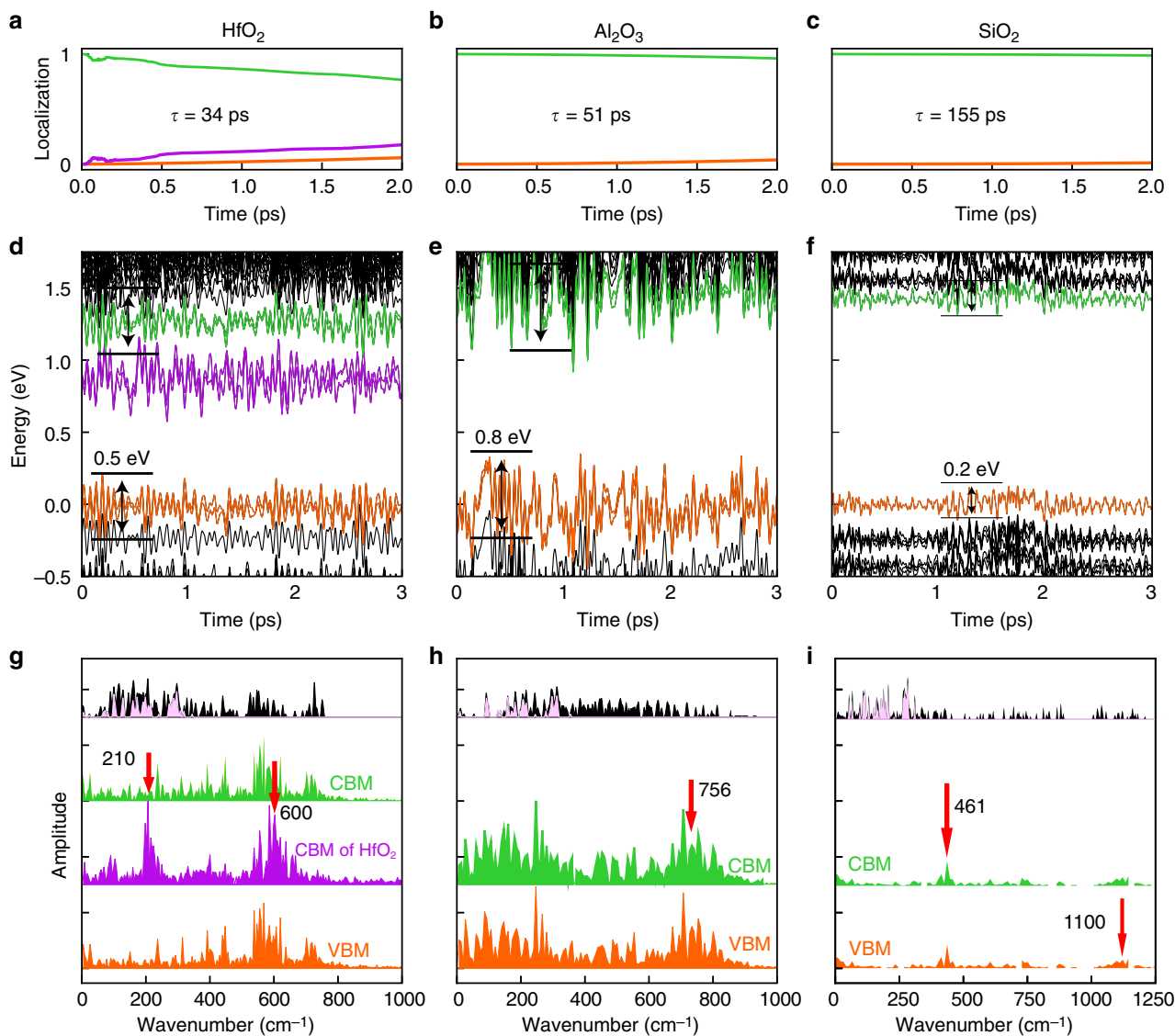
Fig. 3 The non-adiabatic molecular dynamics (NAMD) simulated dynamics of electron–hole (e–h) recombination in monolayers MoSe₂ on HfO₂, Al₂O₃ and SiO₂ substrates. **a–c** The time-dependent electron localization on conduction band minimum (CBM) of MoSe₂. **d–f** The time evolutions of the energy states and **g–i** their corresponding fast Fourier transform (FFT) spectra, where red arrows have marked main phonon modes and its corresponding wavenumbers. The electronic state energy fluctuation amplitude of MoSe₂'s CBM/valence band maximum (VBM) are indicated in **d–f**. The whole phonon DOS of the MoSe₂-oxide substrate systems (black area) and the projection from MoSe₂ (pink area) are also plotted in (**g–i**).

energy difference $\epsilon_k - \epsilon_j$ of the interacting states, the e–ph coupling term $\left\langle \boldsymbol{\varphi}_j | \nabla_R H | \boldsymbol{\varphi}_k \right\rangle$, and the nuclear velocity $\dot{\mathbf{R}}$, which are strongly coupled with phonon excitation. Thus the contribution of phonons plays a crucial role in determining the e–h recombination rate.

To understand the exact role of phonons, time-dependent evolutions of energy levels and their Fourier transform (FT) spectra are displayed in Fig. 3d–i. The electronic states energy fluctuation amplitude is directly related with the e–ph coupling strength and the corresponding FT spectra illustrate the dominant phonon modes and strength involved in the NAMD. First, the electronic state energy fluctuation amplitudes of conduction band minimum/valence band maximum (CBM/VBM) of MoSe₂ are 0.2 eV for SiO₂, 0.8 eV for Al₂O₃ and 0.5 eV for HfO₂, respectively. Smaller amplitude represents weaker e–ph coupling and longer relaxation time, which suggests that the e–ph coupling dominates the observed lifetime modulation. From the phonon DOS and the projection onto MoSe₂ in

Fig. 3g–i, it has been found that the photocarrier/exciton decay in monolayer TMDs is quite susceptible to its phononic environment: MoSe₂ itself mainly contributes to the phonon modes below 400 cm⁻¹ (pink area), while higher frequency phonon modes, participating the interlayer coupling, may come from oxide substrates. Less phonons from SiO₂ contribute to interfacial e–ph coupling, whose strength is weakest. Besides, clean SiO₂ surface is usually unstable and easily gets hydrogenated, which further weakens the interaction between SiO₂ and MoSe₂. Meanwhile, more phonon modes above 400 cm⁻¹ are involved in the recombination process for Al₂O₃ and HfO₂ and their corresponding coupling are much stronger than those on SiO₂. More importantly, these involved phonon modes originate from contributions of oxide substrates. For example, Raman active E_g mode ~756 cm⁻¹ of Al₂O₃ has been observed (Fig. 3h) to be mainly responsible for e–ph coupling[31,49]. In addition, multiphonon hybrid coupling has also been found in Fig. 3g, where the main vibration modes ~600 cm⁻¹ at MoSe₂/HfO₂ interface could arise from the combination of the MoSe₂ A_{1g} mode ~240 cm⁻¹

and the NIR active phonon modes ~337–409 cm^{-1} associated with the vibration of the Hf-O bond[31,50,51]. Furthermore, it should be noted that being different from those of SiO$_2$ and Al$_2$O$_3$, the CBM of HfO$_2$ is located in the bandgap of MoSe$_2$ and this intermediated state also contributes to e–h recombination, because there is an intense phonon mode ~210 cm^{-1} appearing in CBM of HfO$_2$ (purple lines in Fig. 3g), dating from a low-frequency LO phonon mode of HfO$_2$[51]. Thus the phononic environment defined by the oxide substrates plays a dominant role in determining carrier lifetime in monolayer MoSe$_2$.

In principle, the phononic environment discussed above should be related to the substrates' dielectric constant. For a non-metallic solid, the dielectric constant results from the contribution from the ionic and the electronic polarization[50]. In most of the high-κ oxide substrates, the large dielectric constant is due to highly polarizable bonds, especially metal–oxygen bonds. Phonon modes associated with these 'soft' bonds can be easily excited and strongly couple with carriers. Therefore the interfacial e–ph coupling should be positively correlated with dielectric constant and this trend is consistent with our observation, where HfO$_2$ and AlO$_2$ are high-κ materials compared with SiO$_2$.

Discussion

The effect of e–ph coupling at the interface of 2D material and oxide substrates has also been investigated in the context of atomically thin field-effect transistors (FETs)[29,51,52]. In the static transport regime, factors such as Coulomb impurities and defects may serve as additional scattering channels. The dielectric screening effect of high-k substrates are typically used to suppress scattering from Coulomb impurities to increase carrier mobility in TMDs[29,53]. If such screening effect also dominates the photocarrier scattering process, the exciton lifetime in monolayer MoSe$_2$ should be prolonged in HfO$_2$, which is reverse to the observed phenomenon. Thus the overall carrier scattering rate is governed by the combined effects of these factors in a rather complex way. For example, higher dielectric constants are associated with stronger interlayer e–ph coupling coefficients and thus it is an experimental challenge to obtain fully quantitative guidelines to evaluate carrier scattering in different dielectric environments[29,53].

To put our results into the perspective of transport studies of monolayer TMDs, and to also reveal the influence of the dielectric features of the oxide substrates, we repeated the photocarrier lifetime measurements on mechanically exfoliated monolayer MoS$_2$ and MoSe$_2$-based FET devices. A 5-nm ultrathin layer of Al$_2$O$_3$ was deposited on the as-fabricated FET channels (on SiO$_2$/Si substrate) by atomic-layer deposition (ALD), as illustrated in Fig. 4a. Such an experiment allows us to verify the main observations in CVD-grown MoSe$_2$ samples, and also to monitor closely the change of the electrical and optical properties following the formation of the TMD/oxide hybrid system. As revealed by Fig. 4b, the charge-carrier mobility of the MoSe$_2$ channel is found appreciably enhanced after Al$_2$O$_3$ encapsulation, from 6.9 to 9.0 cm^2 V^{-1} S^{-1}, indicating the presence of strong dielectric screening effect. On the other hand, broadband transient measurements (pump = 500 nm, probe = 790 and 765 nm) were used to reveal the exciton lifetime. Clearly, the same exciton lifetime reduction trend as observed with the CVD-MoSe$_2$/oxide samples is reproduced, as shown in Fig. 4c, d. This makes sense as the interlayer e–ph coupling is a generic effect that has been experimentally observed in a range of TMDs materials. For the MoS$_2$ flake, a mobility increase from 13.3 to 23.0 cm^2 V^{-1} S^{-1} and clear lifetime reduction are also observed (Supplementary Fig. 11). These observations suggest that, compared with the static transport scenario, exciton scattering at the monolayer

TMD/dielectric interface could follow a much simpler physical picture, where interfacial e–ph coupling represents the main energy relaxation channel at room temperature. In fact, under room temperature, the dominance of e–ph coupling as the energy dissipation route has also been observed in other 2D materials, such as graphene[32,54].

In summary, through interface engineering we demonstrated an effective way to manipulate the exciton lifetimes of monolayer TMDs at room temperature. Theoretical simulations based on NAMD approach has identified specific phonon modes from the substrates that are coupled to photocarriers in MoSe$_2$ to accelerate the e–h recombination. Such an approach is inherently desirable as most optoelectronic devices involve depositing TMDs or TMD-based heterostructures atop or between gate dielectrics. It is also exciting as the emerging phenomenon of interlayer e–ph coupling in heterostructures made of 2D constituents can be immediately useful[30,31]. With the vast possibility with interfacial phonic environments provided by van der Waals heterostructures, deterministic control of photocarrier dynamics may be realized. Our findings highlight the importance of interlayer e–ph interaction as a mechanism for manipulating the fundamental optical properties of 2D semiconductors, and open up a fabrication-compatible degree of freedom for optimizing TMD-based optoelectronic device.

Method

Sample fabrication. Single crystal monolayer MoSe$_2$ was grown on SiO$_2$/Si substrates by CVD method. After growth, the monolayer MoSe$_2$ was transferred onto different substrates, where different oxide layers (SiO$_2$, Al$_2$O$_3$ and HfO$_2$) were grown on p-doped Si substrates by ALD. For the transfer process, the chip was first coated with a water-soluble polymer polyvinylpyrrolidone (PVP), which served as the adhesive layer. After heating the chip for 1 min at 75 °C, another water-soluble support layer, polyvinyl alcohol (PVA), was dropped onto the PVP film and heated for drying. Then the film was peeled off from the chip and pasted onto other substrates. Finally, the polymers were removed by soaking in water at 80 °C for ~20 min.

The MoS$_2$ and MoSe$_2$ flakes were prepared by standard mechanical exfoliation method, then deposited on a Si/SiO$_2$ (285 nm) wafer. To avoid any organic residue, the Au patches as source/drain contact electrodes were mechanically transferred onto the exfoliated MoS$_2$ and MoSe$_2$ flakes. To verify the influence of oxide layers, high-permittivity Al$_2$O$_3$ layers (5 nm thick) were then deposited on the entire device to form insulating layers. The Al$_2$O$_3$ layers were grown by ALD using trimethylaluminum (TMA)/water precursors without any pre-treatment. The grown rate of Al$_2$O$_3$ deposition was ~1 Å per cycle, where one cycle was ~60 s. The deposition process was carried out at 150 °C to ensure the high quality of Al$_2$O$_3$ film.

Differential reflection measurements. Probing of the transient photo-response of monolayer TMDs on different substrates was carried out using a custom-built pump-probe setup, shown in Supplementary Fig. 3. For this setup, a 76-MHz mode-locked Ti:Sapphire laser is used to generate 100 fs pulse with central wavelengths in the range of 740–900 nm. A large portion (~90%) of the laser power is focused on a beta barium borate crystal to generate the high photon-energy pump beam, which excite carriers in the conduction band. The rest of laser beam works as the probe and its wavelength is chosen to coincide with the bandgap of monolayer MoSe$_2$ (MoS$_2$). By adopting a ×10 microscope objective lens, the pump and probe beams are tightly focused on the TMDs flakes and the diameter of spot size is about 15 μm, appreciably smaller than the dimension of the samples. For a certain measurement, a pump beam with high photon energy inject photocarriers/excitons into the samples and the status of the samples is monitored by measuring the differential reflection signals of the probe beam after a filter blocking the pump beam. The measured signal is the relative change of probe beam reflection.

Time-resolved photoluminescence. The PL lifetimes of photocarriers under room temperature have been measured by a spectroscopy system (from Andor Inc.), equipped with a streak camera. The excitation laser was 405 nm and then the excited PL signals were collected by a lens. A spectrometer with a grating and a slit can efficiently separate the PL signal from the excitation laser, and the output PL signal can be detected by a streak camera, whose instrumental resolution is 32 ps. In addition, the low-temperature TR-PL of samples were measured in a cryostation, and the sample temperature was set at 5 K. the excitation source was 726-nm pulsed diode laser and a long-pass filter was used to block the fundamental laser. Transmitted PL signals were detected by a streak camera.
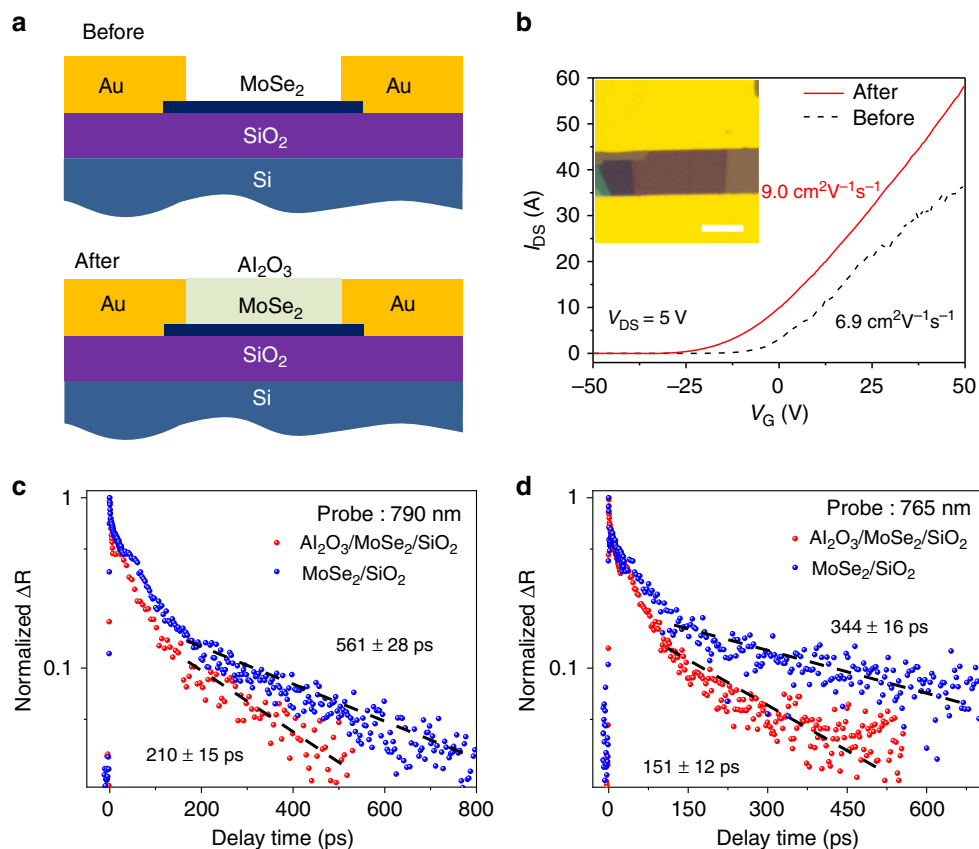
Fig. 4 Electrical transport and photocarrier dynamics of exfoliated monolayer MoSe$_2$ before and after oxide layer deposition. a Schematic illustration of a monolayer MoSe$_2$ field-effect transistor device before and after Al$_2$O$_3$ encapsulation. The Al$_2$O$_3$ layer is ~5 nm thick and deposited by atomic-layer deposition (not drawn to proportion). **b** Source-drain current I_{DS} as a function of the back-gate voltage V_G. The charge mobility inferred before and after Al$_2$O$_3$ encapsulation are 6.9 and 9.0 cm^2 V^{-1} S^{-1}, respectively. Inset shows the optical micrograph of the device, where the scale bar is 20 μm. **c**, **d** Normalized transient reflectance signals before and after Al$_2$O$_3$ encapsulation under different probe wavelengths when pump beam is fixed at 500 nm. The existence of Al$_2$O$_3$ makes the lifetime of photocarrier reduce regardless of probe wavelength

Data availability

References

1. Yin, X. et al. Edge nonlinear optics on a MoS$_2$ atomic monolayer. *Science* **344**, 488–490 (2014).
2. Mak, K. F., Lee, C., Hone, J., Shan, J. & Heinz, T. F. Atomically thin MoS$_2$: a new direct-gap semiconductor. *Phys. Rev. Lett.* **105**, 136805 (2010).
3. Radisavljevic, B., Radenovic, A., Brivio, J., Giacometti, V. & Kis, A. Single-layer MoS$_2$ transistors. *Nat. Nanotechnol.* **6**, 147–150 (2011).
4. Wang, Q. H., Kalantar-Zadeh, K., Kis, A., Coleman, J. N. & Strano, M. S. Electronics and optoelectronics of two-dimensional transition metal dichalcogenides. *Nat. Nanotechnol.* **7**, 699–712 (2012).
5. Splendiani, A. et al. Emerging photoluminescence in monolayer MoS$_2$. *Nano Lett.* **10**, 1271–1275 (2010).
6. Zhang, Y. et al. Direct observation of the transition from indirect to direct bandgap in atomically thin epitaxial MoSe$_2$. *Nat. Nanotechnol.* **9**, 111–115 (2014).
7. Mak, K. F. et al. Tightly bound trions in monolayer MoS$_2$. *Nat. Mater.* **12**, 207–211 (2013).
8. Ugeda, M. M. et al. Giant bandgap renormalization and excitonic effects in a monolayer transition metal dichalcogenide semiconductor. *Nat. Mater.* **13**, 1091–1095 (2014).
9. Amani, M. et al. Near-unity photoluminescence quantum yield in MoS$_2$. *Science* **350**, 1065–1068 (2015).
10. Lei, S. et al. Surface functionalization of two-dimensional metal chalcogenides by Lewis acid-base chemistry. *Nat. Nanotechnol.* **11**, 465–471 (2016).
11. Lopez-Sanchez, O., Lembke, D., Kayci, M., Radenovic, A. & Kis, A. Ultrasensitive photodetectors based on monolayer MoS$_2$. *Nat. Nanotechnol.* **8**, 497–501 (2013).
12. Ross, J. S. et al. Electrically tunable excitonic light-emitting diodes based on monolayer WSe$_2$ p-n junctions. *Nat. Nanotechnol.* **9**, 268–272 (2014).
13. Ye, Y. et al. Monolayer excitonic laser. *Nat. Photonics* **9**, 733–737 (2015).
14. Sun, Z., Martinez, A. & Wang, F. Optical modulators with 2D layered materials. *Nat. Photonics* **10**, 227–238 (2016).
15. Wang, H., Zhang, C., Chan, W., Tiwari, S. & Rana, F. Ultrafast response of monolayer molybdenum disulfide photodetectors. *Nat. Commun.* **6**, 8831 (2015).
16. Korn, T., Heydrich, S., Hirmer, M., Schmutzler, J. & Schüller, C. Low-temperature photocarrier dynamics in monolayer MoS$_2$. *Appl. Phys. Lett.* **99**, 102109 (2011).
17. Shi, H. et al. Exciton dynamics in suspended monolayer and few-layer MoS$_2$ 2D crystals. *ACS Nano* **7**, 1072–1080 (2013).
18. Docherty, C. J. et al. Ultrafast transient terahertz conductivity of monolayer MoS$_2$ and WSe$_2$ grown by chemical vapor deposition. *ACS Nano* **8**, 11147–11153 (2014).
19. Kumar, N. et al. Exciton-exciton annihilation in MoSe$_2$ monolayers. *Phys. Rev. B* **89**, 125427 (2014).
20. Nie, Z. et al. Ultrafast carrier thermalization and cooling dynamics in few-layer MoS$_2$. *ACS Nano* **8**, 10931–10940 (2014).
21. Chernikov, A., Ruppert, C., Hill, H. M., Rigosi, A. F. & Heinz, T. F. Population inversion and giant bandgap renormalization in atomically thin WS$_2$ layers. *Nat. Photonics* **9**, 466–470 (2015).
22. Dey, P. et al. Optical coherence in atomic-monolayer transition-metal dichalcogenides limited by electron-phonon interactions. *Phys. Rev. Lett.* **116**, 127402 (2016).

23. Wang, H., Zhang, C. & Rana, F. Surface recombination limited lifetimes of photoexcited carriers in few-layer transition metal dichalcogenide MoS₂. *Nano Lett.* **15**, 8204–8210 (2015).

24. Li, Y. et al. Effects of rhenium dopants on photocarrier dynamics and optical properties of monolayer, few-layer, and bulk MoS₂. *Nanoscale* **9**, 19360–19366 (2017).

25. Siegner, U., Fluck, R., Zhang, G. & Keller, U. Ultrafast high-intensity nonlinear absorption dynamics in low-temperature grown gallium arsenide. *Appl. Phys. Lett.* **69**, 2566–2568 (1996).

26. Lederer, M. J., Luther-Davies, B., Tan, H. H. & Jagadish, C. GaAs based anti-resonant Fabry–Perot saturable absorber fabricated by metal organic vapor phase epitaxy and ion implantation. *Appl. Phys. Lett.* **70**, 3428–3430 (1997).

27. Keller, U. Recent developments in compact ultrafast lasers. *Nature* **424**, 831 (2003).

28. Zhu, C. et al. A robust and tuneable mid-infrared optical switch enabled by bulk Dirac fermions. *Nat. Commun.* **8**, 14111 (2017).

29. Zou, K., Hong, X., Keefer, D. & Zhu, J. Deposition of high-quality HfO₂ on graphene and the effect of remote oxide phonon scattering. *Phys. Rev. Lett.* **105**, 126601 (2010).

30. Jin, C. et al. Interlayer electron–phonon coupling in WSe₂/hBN heterostructures. *Nat. Phys.* **13**, 127–131 (2016).

31. Chow, C. M. et al. Unusual exciton-phonon interactions at van der Waals engineered interfaces. *Nano Lett.* **17**, 1194–1199 (2017).

32. Gao, B. et al. Studies of intrinsic hot phonon dynamics in suspended graphene by transient absorption microscopy. *Nano Lett.* **11**, 3184–3189 (2011).

33. Lin, Y. et al. Dielectric screening of excitons and trions in single-layer MoS₂. *Nano Lett.* **14**, 5569–5576 (2014).

34. Tonndorf, P. et al. Photoluminescence emission and Raman response of monolayer MoS₂, MoSe₂, and WSe₂. *Opt. Express* **21**, 4908–4916 (2013).

35. Liu, H.-L. et al. Optical properties of monolayer transition metal dichalcogenides probed by spectroscopic ellipsometry. *Appl. Phys. Lett.* **105**, 201905 (2014).

36. Wang, H., Zhang, C. & Rana, F. Ultrafast dynamics of defect-assisted electron-hole recombination in monolayer MoS₂. *Nano Lett.* **15**, 339–345 (2015).

37. Steinleitner, P. et al. Direct observation of ultrafast exciton formation in a monolayer of WSe₂. *Nano Lett.* **17**, 1455–1460 (2017).

38. Ceballos, F., Cui, Q., Bellus, M. Z. & Zhao, H. Exciton formation in monolayer transition metal dichalcogenides. *Nanoscale* **8**, 11681–11688 (2016).

39. Selig, M. et al. Dark and bright exciton formation, thermalization, and photoluminescence in monolayer transition metal dichalcogenides. *2D Mater.* **5**, 035017 (2018).

40. Yu, Y. et al. Fundamental limits of exciton-exciton annihilation for light emission in transition metal dichalcogenide monolayers. *Phys. Rev. B* **93**, 201111 (2016).

41. Hoshi, Y. et al. Suppression of exciton-exciton annihilation in tungsten disulfide monolayers encapsulated by hexagonal boron nitrides. *Phys. Rev. B* **95**, 241403 (2017).

42. Raja, A. et al. Coulomb engineering of the bandgap and excitons in two-dimensional materials. *Nat. Commun.* **8**, 15251 (2017).

43. Yuan, L. & Huang, L. Exciton dynamics and annihilation in WS₂ 2D semiconductors. *Nanoscale* **7**, 7402–7408 (2015).

44. Robert, C. et al. Exciton radiative lifetime in transition metal dichalcogenide monolayers. *Phys. Rev. B* **93**, 205423 (2016).

45. Zhang, Y., Tan, Y.-W., Stormer, H. L. & Kim, P. Experimental observation of the quantum Hall effect and Berry's phase in graphene. *Nature* **438**, 201 (2005).

46. Kresse, G. & Hafner, J. Ab initio molecular dynamics for liquid metals. *Phys. Rev. B* **47**, 558 (1993).

47. Kresse, G. & Furthmüller, J. Efficient iterative schemes for ab initio total-energy calculations using a plane-wave basis set. *Phys. Rev. B* **54**, 11169 (1996).

48. Zhang, L., Vasenko, A. S., Zhao, J. & Prezhdo, O. V. Mono-elemental properties of 2D black phosphorus ensure extended charge carrier lifetimes under oxidation: time-domain ab initio analysis. *J. Phys. Chem. Lett.* **10**, 1083–1091 (2019).

49. Cataliotti, R. Phonon spectrum and phonon interactions in corundum. *J. Phys. C* **7**, 3467 (1974).

50. Fischetti, M. V., Neumayer, D. A. & Cartier, E. A. Effective electron mobility in Si inversion layers in metal–oxide–semiconductor systems with a high-κ insulator: the role of remote phonon scattering. *J. Appl. Phys.* **90**, 4587–4608 (2001).

51. Desgreniers, S. & Lagarec, K. High-density ZrO₂ and HfO₂: crystalline structures and equations of state. *Phys. Rev. B* **59**, 8467 (1999).

52. Yu, Z. et al. Realization of room-temperature phonon-limited carrier transport in monolayer MoS₂ by dielectric and carrier screening. *Adv. Mater.* **28**, 547–552 (2016).

53. Cui, Y. et al. High-performance monolayer WS₂ field-effect transistors on high-kappa dielectrics. *Adv. Mater.* **27**, 5230–5234 (2015).

54. Tielrooij, K. J. et al. Out-of-plane heat transfer in van der Waals stacks through electron-hyperbolic phonon coupling. *Nat. Nanotechnol.* **13**, 41–46 (2018).

Acknowledgements

Author contributions

F.W. and J.Z. conceived the project and together with R.Z., Y.S. and Y.X., supervised the project. Y.M. and F.S. prepared the CVD-MoSe₂ samples. Z.N., Y.W. and S.Q. performed the ultrafast pump-probe experiments. Y.C. and H.J. prepared the mechanically exfoliated MoS₂ and MoSe₂ as well as the ALD deposition of oxides. Xiaoyong W. contributed to the time-resolved PL measurement. Y.S., Q.Z. and J.Z. performed the theoretical calculations. Xinran W. and I.C.E.T. provided help with experimental analysis. F.W., J.Z. and R.Z. wrote the paper with all authors contributing to discussion and preparation of the manuscript.

Additional information

Competing interests: The authors declare no competing interests.

Reprints and permission information is available online at http://npg.nature.com/reprintsandpermissions/

Publisher's note: Springer Nature remains neutral with regard to jurisdictional claims in published maps and institutional affiliations.